Band Gap Engineering of Chemical Vapor Deposited Graphene by *in Situ* BN Doping

Cheng-Kai Chang,[†,‡] Satender Kataria,[†,§] Chun-Chiang Kuo,[†] Abhijit Ganguly,[⊥] Bo-Yao Wang,[¶,#] Jeong-Yuan Hwang,[⊥] Kay-Jay Huang,[▽] Wei-Hsun Yang,[■] Sheng-Bo Wang,[▲] Cheng-Hao Chuang,[¶,#] Mi Chen,[▽] Ching-I Huang,[‡] Way-Faung Pong,[¶] Ker-Jar Song,[†] Shoou-Jinn Chang,[▲] Jing-Hua Guo,[#] Yian Tai,[■] Masahiko Tsujimoto,[○] Seiji Isoda,[+] Chun-Wei Chen,[§] Li-Chyong Chen,[⊥,*] and Kuei-Hsien Chen[†,⊥,*]

[†]Institute of Atomic and Molecular Sciences, Academia Sinica, Taipei, 10617, Taiwan, [‡]Institute of Polymer Science and Engineering, [§]Department of Materials Science and Engineering, and [⊥]Center for Condensed Matter Sciences, National Taiwan University, Taipei, 10617, Taiwan, [¶]Department of Physics, Tamkang University, Tamsui, 251, Taiwan, [#]Advanced Light Source, Lawrence Berkeley National Laboratory, Berkeley, California 94720, United States, [▽]Department of Chemical and Materials Engineering, Minghsin University of Science and Technology, Hsinchu, 30401, Taiwan, [■]Department of Chemical Engineering, National Taiwan University of Science and Technology, Taipei, 10607, Taiwan, [▲]Institute of Microelectronics and Department of Electrical Engineering, National Cheng Kung University, Tainan, 70101, Taiwan, [○]Institute for Chemical Research, Kyoto University, Kyoto 611-0011, Japan, and [+]Institute for Integrated Cell-Material Sciences, Kyoto Universty, Kyoto 606-8501, Japan

ABSTRACT Band gap opening and engineering is one of the high priority goals in the development of graphene electronics. Here, we report on the opening and scaling of band gap in BN doped graphene (BNG) films grown by low-pressure chemical vapor deposition method. High resolution transmission electron microscopy is employed to resolve the graphene and h-BN domain formation in great detail. X-ray photoelectron, micro-Raman, and UV−vis spectroscopy studies revealed a distinct structural and phase evolution in BNG films at low BN concentration. Synchrotron radiation based XAS-XES measurements concluded a gap opening in BNG films, which is also confirmed by field effect transistor measurements. For the first time, a significant band gap as high as 600 meV is observed for low BN concentrations and is attributed to the opening of the $\pi-\pi^*$ band gap of graphene due to isoelectronic BN doping. As-grown films exhibit structural evolution from homogeneously dispersed small BN clusters to large sized BN domains with embedded diminutive graphene domains. The evolution is described in terms of competitive growth among h-BN and graphene domains with increasing BN concentration. The present results pave way for the development of band gap engineered BN doped graphene-based devices.

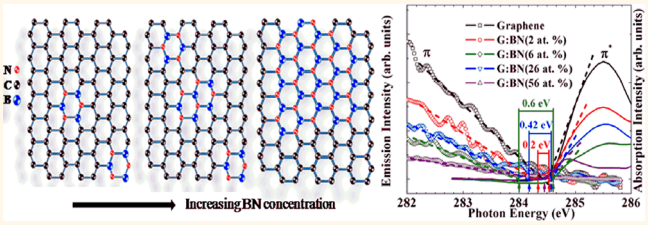

KEYWORDS: BN doping · graphene · chemical vapor deposition · band gap · XPS · micro-Raman · XAS-XES

The astonishing physical properties of graphene-like high optical transparency, superior mechanical strength, and excellent charge carrier mobility make it a suitable candidate for device applications which include electronics, optoelectronics, photonics, and spintronics.[1−8] However, the absence of a band gap limits its implementation to device applications especially in graphene-based electronics. A number of theoretical and experimental approaches have been demonstrated to tailor the graphene electronic structure for opening up a band gap. The main methods include quantum confinement of charge carriers from 2D to 1D in graphene nanoribbons,[9−11] controlling the stacking geometry in bilayer graphene,[12] chemical doping,[13−15] and application of strain.[16,17] Nevertheless, toward commercialization, several bottlenecks remain to be solved in each method, such as a lack of chirality control and scalability during fabrication of graphene nanoribbons, difficulties of producing large-area bilayer graphene with controlled stacking, and insufficient quality of crystallization.

Out of the methods described above, chemical doping of graphene seems to be most promising. Shi *et al.*[13] have demonstrated a tunable work function in chemically doped graphene. D. Usachov *et al.*[15] have synthesized N-doped graphene by the chemical vapor deposition (CVD) method. Using *in situ* photoelectron spectroscopy

* Address correspondence to chenkh@pub.iams.sinica.edu.tw, chenlc@ ntu.edu.tw.

Received for review October 23, 2012 and accepted December 29, 2012.

Published online December 30, 2012
10.1021/nn3049158

studies, they are able to show a band gap opening of 0.2 eV in N-doped graphene. Theoretically, it has been predicted that one can manipulate the electronic band structure of graphene by codoping with boron and nitrogen atoms which may lead to the band gap opening of graphene.[18−22]

Recent reports on the synthesis of large-area few-layer hexagonal BN (*h*-BN) using a CVD process have stimulated research on codoping B and N in graphene.[23,24] Ci *et al.*[25] have synthesized atomic layers of hybrid *h*-BN and graphene domains, and the resultant films exhibited semiconducting behavior with a small band gap of around 18 meV due to the carrier confinement within the "graphene paths" embedded in BN domains. It is to be mentioned here that the authors have reported the synthesis for BN concentrations higher than 10% where BN segregation has already occurred. However, so far there is no concrete experimental demonstration that a small amount of well distributed h-BN domains in graphene shows the electronic structure with a significant band gap, as predicted through theoretical studies.

RESULTS AND DISCUSSION

Here, we report the synthesis of large-area, few-layer BN codoped graphene (BNG) using a low pressure CVD method on Cu foils. The present study is mainly focused on low BN concentration in graphene unlike the previous report[25] where hybridized h-BN and graphene domains are formed at high BN concentrations. Figure 1 shows the schematic of experimental set up and methodology adopted and is detailed in the Methods section. The experimental setup is established for growing large area graphene samples using CH_4 gas as the carbon source.[26] For the growth of BNG films, ammonia borane precursor is used as the BN source and is introduced as vapor during graphene growth. The BN content in the graphene layers can be varied by controlling the heating temperature of the precursor. X-ray photoelectron spectroscopy (XPS) studies have confirmed a monotonic increase in BN content with a rise in heating temperature of the precursor. Here, we employ X-ray absorption (XAS) and emission (XES) spectroscopic studies to reveal the influence of BN doping on the electronic structure of graphene.

Elemental composition of the as grown pristine graphene and BNG films was determined using XPS. No B and N peaks were detected for pristine graphene. Samples are designated according to the elemental composition obtained by XPS analysis; for example, 2BNG stands for 2% BN-doped graphene film. Figure 2 panels a−c show the typical XPS spectra of C, N, and B peaks, respectively, for as grown 8BNG films where BN concentration is around 8%. As shown in Figure 2a, the C 1s spectrum can be deconvoluted into four peaks, that is, C_1−C_4 with main intense peak C_1 centered at around 284.5 eV, which corresponds to C−C sp^2 bonds depicting the graphitic nature of C atoms. The other less intense peaks C_2−C_4 situated between 285.5 and 288.6 eV are attributed to C−N bonds.[27] Interestingly, we did not observe any peak corresponding to B−C bonds in any of our BNG films, which are generally claimed to be at lower binding energy side.[28] The possible reason for the same is described later while discussing the structural evolution in BNG films. Figure 2b shows the N 1s spectrum for the 8BNG sample which is very well discriminated into a two-peak feature. The peak N_B at 398 eV is attributed to the presence of N−B bonds[27] and the small peak N_C around 399.5 eV is due to the presence of N−C bonding configurations.[28,29] This is in corroboration with C 1s spectra where peaks corresponding to different configurations of C and N bonds are observed (Figure 2a). In contrast, the XPS spectrum of B for 8BNG film exhibited a single peak centered at around 190.5 eV, as depicted in Figure 2c, which can be assigned to B−N bonds and matches well with the B peak in the h-BN phase.[30,31] The appearance of a peak at 398 eV in the N 1s spectrum and a 190.5 eV peak in the B 1s spectrum correlates well with previously reported values for few-layer h-BN films.[30] No peak corresponding to B−C bonds was observed in the B 1s spectra. It should be mentioned here that a B signal was not detected by XPS and even by electron energy loss spectroscopy (EELS) in low BN concentration samples, that is, 2BNG and 6BNG, owing to the low atomic sensitivity of B. This is in corroboration with N 1s spectra where a peak related to the N−B bonds was observed initially for 8BNG only (Figure 2d). To confirm the presence of B in 2BNG and 6BNG samples, we have employed the Auger electron spectroscopy (AES) technique, wherein both B and N signals were detected with similar intensity, indicating that the B and N atomic ratio is 1 in the samples (see Supporting Information, Figure S1). Further evidence is provided by the distinct evolution of N 1s spectra with increasing BN concentration, as shown in Figure 2d. It is observed that the peak N_B at 398 eV is evolving and the peak N_C at 399.5 eV is diminishing with increase in BN concentration. The N_B peak is not detected in the case of 2BNG and 6BNG films, but the N_C peak is clearly observed. However, the N_B peak starts appearing distinctly for the 8BNG film and at this stage the N 1s spectra can be deconvoluted into two distinct peaks (Figure 2b). With a further increase in BN concentration, a gradual rise of the N_B peak intensity with a simultaneous decrease in the N_C peak intensity is observed which can be directly related to the increasing numbers of N−B bonds over N−C bonds. This indicates toward the preferential bonding between N and B atoms leading to an increased number of BN domains. Therefore, it can be concluded that h-BN domains are getting incorporated in graphene as BN concentration is increasing and is evidenced by B 1s and N 1s spectra where peaks related to h-BN phase are observed. However, h-BN domains could be so diluted in 2BNG and 6BNG films that no signature of B−N bonds is observed in B1s and N1s

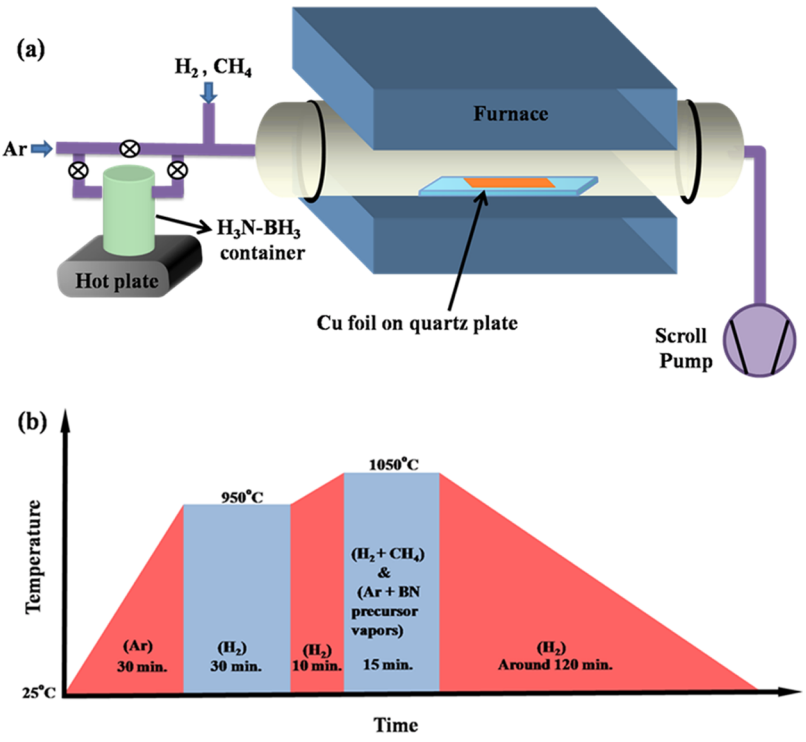

Figure 1. (a) Schematic diagram of the experimental setup used in the present study. (b) Methodology used for the deposition of BNG films.

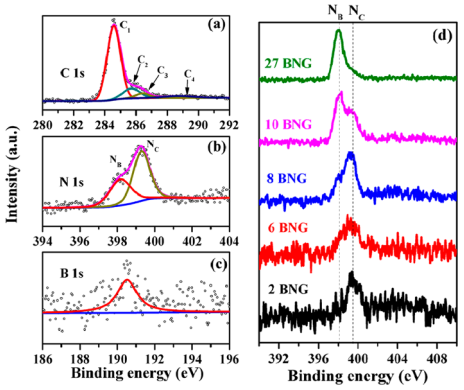

Figure 2. Typical XPS spectra of (a) C 1s, (b) N 1s, and (c) B 1s core levels for 8BNG film. The empty circles are raw data and solid lines are the fitted spectra. (d) N 1s spectra for different BNG films as a function of increasing BN concentration. Dashed lines are guide to eyes.

XPS spectra. We should mention here that XPS sensitivity for B is low as compared to that for C and N, and therefore B−N bonds are not detected in 2BNG and 6BNG films. However, the presence of B and N in 2BNG film is confirmed by AES (see Supporting Information, Figure S1). High resolution XAS spectra obtained by synchrotron radaitions also confirms the presence of B−N bonds in the films (see Supporting Information, Figure S2). The evolution of BN domains is also confirmed by Raman studies, as elaborated later, where the h-BN phase is found to appear at higher BN concentrations.

Figure 3 shows the Raman spectrum of as-grown pristine graphene and BNG samples. Raman measurements confirmed the formation of single layer graphene with characteristic G and 2D bands at around 1585 and 2645 cm^{-1}, respectively, with an I_{2D}/I_G ratio around 4. A significant shift of the 2D band is observed with an increase in BN concentration. Initially, the 2D band downshifts up to 2634 cm^{-1} for the 6BNG sample and then it exhibits an upshift up to 2649 cm^{-1} for the 8BNG sample. The shift in the 2D band for BN concentrations up to 6% could be due to a doping effect as this effect is more pronounced for low doping levels.[32] However, as BN domains segregate out of the graphene matrix in the case of the 8BNG sample (as revealed by XPS and TEM studies), the effect of the strained graphene lattice may dominate resulting in the observed upshift of the 2D band. A barely discernible D band was observed in pristine graphene indicating the excellent quality of the sample. With increasing BN content during graphene growth, a significantly intense D band at around 1325 cm^{-1} was found to appear in the Raman spectra. The presence of the D band indicates the induction of defects in the crystalline graphene lattice.[33] Another disorder induced band D′ also appeared at around 1620 cm^{-1} for samples containing higher BN content. Further increase in the BN content led to an increase in I_D/I_G ratio as listed in Table 1. Raman area mapping of the I_D/I_G ratio was conducted for BNG samples. Raman spatial maps were obtained by raster scanning the samples in the *X* and *Y* directions using a high precision stage. The laser beam was focused to a spot size of 1 μm. Raman maps for 2BNG and 6BNG films are shown in Figure 3 panels b and

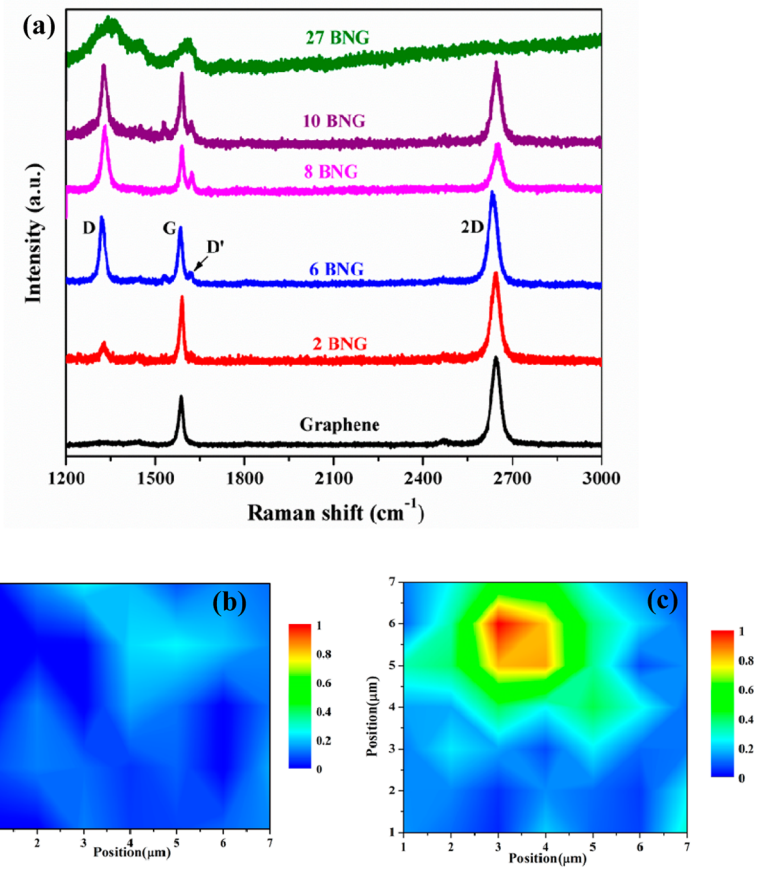

Figure 3. (a) Raman spectra of BNG films acquired using 633 nm wavelength laser. Raman area mapping of I_D/I_G ratio for (b) 2BNG and (c) 6BNG films.

TABLE 1. Defect Density and Crystallite Size in BNG Films Calculated Using I_D/I_G Ratio Obtained from Raman Spectra

sample	I_D/I_G	defect density ($\times 10^{10}$ cm^{-2})	graphene crystallite size (nm)
graphene	0.11	1.24	348
2BNG	0.26	2.93	147
6BNG	1.5	16.92	25.5
8BNG	2.7	30.46	14.2
10BNG	1.8	19.74	21.3

c, respectively. Defect density and graphene crystallite size were also determined using the I_D/I_G ratio.[34,35] A significant defect density of the order of 10^{10} cm^{-2} was determined for pristine graphene and can be attributed to one-dimensional defects like grain boundaries and other structural defects which are unavoidable in CVD graphene owing to the use of polycrystalline Cu foils as catalyst. With the incorporation of BN during graphene growth, defect density was found to increase significantly as compared to pristine graphene. For the 2BNG sample, defect density was around 2.5 times higher as compared to pristine graphene and an order of magnitude increase was observed for films with BN concentration greater than 6%. Assuming that pristine graphene has a larger grain size, we can attribute the increase in defect density to the formation of a BN cluster which restricts the growth of graphene domains, leading to an increased number of grain boundaries in BNG films. This is further evidenced by a decrease in graphene crystallite size where pristine graphene exhibited a crystallite size of around 348 nm (Table 1), and with the inclusion of BN in graphene, crystallite size was found to decrease at the same rate with which defect density was increasing. This observation points toward a direct correlation among defect density and crystallite size in BNG films, which can have a direct impact on the mobility of charge carriers in the samples. Also, the I_{2D}/I_G ratio decreased from 4 to 2.5 for the 10BNG sample. Interestingly, for 27BNG sample with 27% BN content, the 2D band completely disappeared and two broad bands centered around 1300 and 1600 cm^{-1} were observed in the visible Raman spectra. To explore the Raman characteristic of BN domains, UV-Raman measurements using 325 nm laser wavelength have been implemented. A sharp peak at around 1370 cm^{-1} corresponding to the E_{2g} mode of the h-BN phase was observed[36] for 27BNG films (see Supporting Information, Figure S3) along with a broad peak around 1600 cm^{-1}. This points toward the formation of the h-BN phase which is well corroborated by XPS studies where peaks corresponding to B−N bonds are observed in B and N spectra for high-concentration BNG films.

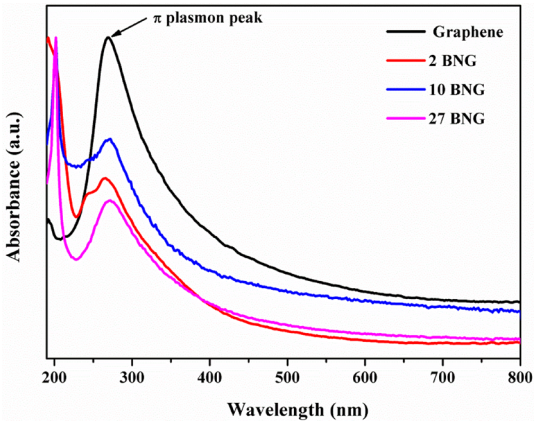

Figure 4. UV−vis spectra for different BNG films depicting the evolution of the h-BN phase.

UV−vis studies have also been carried out in order to further understand the optical properties of as-grown BNG films. Figure 4 shows the spectra for pristine graphene and BNG films. A broad absorption peak around 268 nm (4.6 eV) is observed in the case of pristine graphene and is attributed to resonant excitonic effects due to electron−hole interaction in the π and π^* bands at the M point.[37] The intensity of π plasmon peak is found to decrease with increasing BN concentration and a broad hump at around 200 nm appears and becomes a sharp peak and dominates the spectra. This peak at around 200 nm corresponds to the optical absorption gap energy of the h-BN phase.[25] This evolution in UV−vis spectra of BNG films reveals and confirms the formation and segregation of h-BN domains at higher BN concentrations, where the presence of characteristic π plasmon peak of graphene (at 268 nm) further attests the existence of graphene domains. It should be mentioned here that UV−vis spectra cannot be exploited to determine the band gap of BNG films owing to the absence of a band absorption edge in graphene; however, one can trace the band edge absorption of h-BN (see Supporting Information, Figure S4). With an increase in BN concentration, the optical band gap corresponding to the h-BN phase was found to increase toward the bulk value of h-BN. Therefore, we have employed the XES-XAS technique to gain insights in the band gap of BNG films, as discussed later.

The BNG samples were further characterized using transmission electron microscopy (TEM), selective area diffraction pattern (SAED), and electron energy loss spectroscopy (EELS) (see Supporting Information, section S5). TEM observations revealed that BNG films were dominantly 1−2 layers, as shown in Figure 5a. Interestingly, we did not observe BN crystallites in 2BNG sample as depicted in Figure 5b where only graphene domains were observed. Moreover, B and N were not detected in 2BNG film by EELS (see Supporting Information, Figure S5a). However, finely distributed BN domains of a size around 2−10 nm were observed in 8BNG film, as shown in Figure 5c where the B and N K edge peaks were also detected, though with small intensity during EELS analysis (see Supporting Information, Figure S5b). TEM observations are in line with XPS results where segregation of the BN domains is found to occur for 8BNG film with 8% BN content in graphene. Therefore, it can be concluded from TEM studies that BN clusters present in 2BNG and 6BNG films are very much diluted and homogeneously distributed in the graphene lattice and have significant effect on the optical properties as revealed by Raman and UV−vis studies. However, an increase in BN concentration above 8% results in the formation of well-segregated BN domains during graphene growth and leads to hybridized structure consisting of h-BN and graphene domains. The present findings are in line with the previous report[25] where hybridized h-BN and graphene structure is observed for BN concentrations greater than 10%. This is the first observation of structural transformation in BN incorporated graphene films where a transition from dilute BN clusters to well-segregated BN domains is traced. The structural evolution is found to affect the band gap of graphene significantly, as discussed later.

On the basis of the XPS, TEM, and Raman observations mentioned above, we can speculate the structural evolution in the BNG films in the following way. When the ammonia borane precursor is heated, the dehydrogenation process takes place in steps depending on the temperature of the precursor with complete dehydrogenation yielding the BN monomer at high temperatures around 1400−1500 °C.[38] Generally, a temperature range of 60−120 °C is used to vaporize the precursor for the growth of the monolayer or few-layer h-BN films on the Cu surface which is kept at temperatures around 1000 °C.[23,24,39] Monolayer h-BN films are grown on Cu even for a precursor temperature of around 50 °C. However, the h-BN films are not continuous and rather small triangular domains are observed, which increase in size with an increase in precursor temperature.[39] Here, we have used precursor temperatures of more than 60 °C and therefore, the formation of small domains of h-BN cannot be neglected. Hence, the growth of BNG films is actually a competitive growth process between graphene and h-BN domains. To verify this, we have deposited BNG films where the BN precursor temperature is kept constant at 70 °C (corresponding to a BN concentration of 2%) and CH_4 gas flow rate is varied from 5 to 25 sccm. We have observed through XPS that the N peak is diminishing with increasing CH_4 flow rate, indicating the suppression of BN domains growth (see Supporting Information, Figure S6a). Raman measurements have also revealed the dominance of graphene growth, where the D peak is found to disappear and the I_{2D}/I_G ratio is improving with decreasing I_D/I_G ratio (see Supporting Information, Figure S6b). Depending on the concentration of BN and CH_4 gas during the growth, one will obtain BNG films with homogeneously distributed graphene and h-BN domains. At low

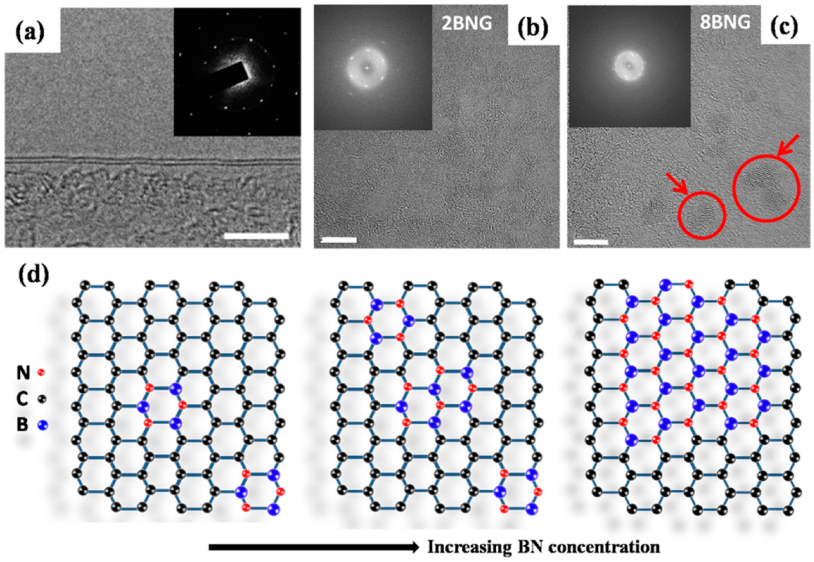

Figure 5. (a) High-resolution TEM image of a BNG film showing the layer number, and the inset represents the electron diffraction pattern taken at the corresponding region. (b) High resolution TEM image of 2BNG sample with fast-Fourier transform (FFT) in the inset showing only graphene crystalline structure. (c) High resolution TEM image of 8BNG sample depicting the distribution of h-BN domains (encircled regions) in graphene. The inset is FFT of the image indicating the presence of crystalline domains of both graphene and h-BN. (Scale bar is 5 nm). (d) Schematic diagram depicting the structural evolution in BNG films with increase in BN concentration. Carbon, nitrogen, and boron atoms are represented by black, red, and blue circles, respectively.

concentrations of BN precursor, graphene growth will dominate with inclusions of small sized and less density of h-BN domains. The dominance will be reversed at high concentrations of BN precursor where h-BN growth is pronounced, as revealed by the Raman studies (Figure 3). The structural evolution is shown by schematics in Figure 5d. It is reported that h-BN domains are mostly terminated with N atoms which is a thermodynamically more favorable configuration.[39] Therefore, it is more likely that graphene and h-BN domains would join through terminated N atoms leading to a B−N−C configuration with N bonded to C atoms. Interestingly, the same has been observed through XPS in the present study, where the presence of different bonding configurations between N and C atoms are attested but no signature of B−C bonds is seen (Figure 2). It should also be mentioned here that even a slight excess of N can result in the formation of N-rich BN domains leading to a greater number of BN−C interfaces.[40] This could probably result in the present observation of N−C bonds but not B−C bonds. Moreover, recent *ab initio* simulations of BN doping in graphene have revealed that formation of h-BN domains is more likely to take place at grain boundaries owing to lower formation energy at the defect regions.[41] The same has been demonstrated quite recently using *in situ* microscopy techniques, where it is observed that BN grows preferentially at the edges of monolayer graphene domains rather than growing on the top of the graphene layer which further substantiates the present observations.[42]

A direct evidence for the band gap opening of low BNG films is provided by the C *K*-edge XAS and K_α XES measurements. Figure 6 panels a and b show the XAS and XES spectra of HOPG, pristine graphene, and BNG samples. For comparison, we have also included the spectra for BNG films with BN concentrations of 26% and 52%. The selected spectra are magnified at the $\pi-\pi^*$ region as shown in Figure 6b for clarity. Both the leading edges of the C *K*-edge XAS and K_α XES spectra have been extrapolated to the baseline in order to determine the conduction-band-minimum and valence-band-maximum, respectively, and the band gap. The two extrapolated lines clearly intersect each other for pristine graphene and films with BN concentration of 52%, meaning that these two samples have no band gap similar to the metallic HOPG. However, in low-BN samples with increasing BN concentration, we have observed a monotonically increasing band gap up to 600 meV for the 6BNG sample. The band gap opening in BN codoped graphene is attributed to the breaking of inherent equivalence of graphene sublattices.[43] The isoelectronic BN doping can effectively open the $\pi-\pi^*$ band gap of graphene as observed in the present study (Figure 6). A further increase in BN concentration leads to a decrease in band gap. This could be correlated with a formation of 2D atomic structures where small graphene domains are surrounded by large-size BN domains. This fact could reduce the above effect, but give rise to a quantum confinement effect in graphene domains, as in the case of graphene nanoribbons, inducing a small band gap in graphene which is less than that observed in low BN concentration samples. Ci *et al.* have reported a band gap of around 18 meV for the sample containing 56% carbon in *h*-BN, and attributed this band gap opening to the

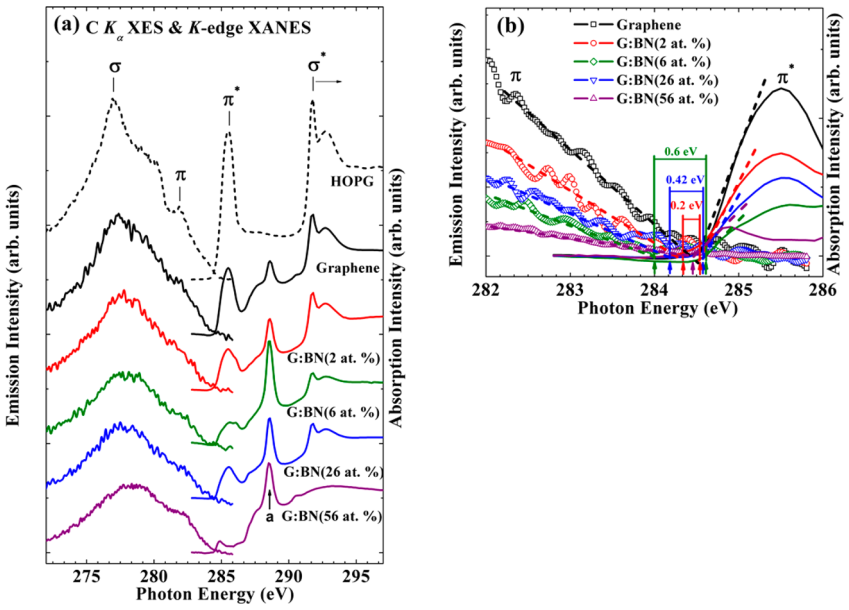

Figure 6. (a) Normalized C *K*-edge XANES and K_α XES spectra of the BNG films (left side, XES; right side, XANES) with various concentrations of B−N doping, pristine graphene, and HOPG. (b) Magnified selected spectra at the $\pi-\pi^*$ region. [Feature "a" present at 288.5 eV could be contributed by either C═N bonding with the B−N dopants, or the C═O/C−OH bonding with the carbonyl group on the surface.]

quantum confinement.[25] The results are quite aligned with the present studies, where a band gap decrease is observed after 6% BN content in graphene. This is the first report on a significant band gap opening in graphene hybridized with small and diluted domains of h-BN.

Graphene and BNG samples were successfully transferred to SiO_2 substrates for electrical characterization. BN doping of graphene has a pronounced effect on the transport properties and resistance of pristine graphene. Figure 7a shows the resistance *versus* temperature curve for pristine graphene and 2BNG film. The pristine graphene shows ideal semimetallic behavior with zero or small energy gap. No change in resistance was observed for pristine graphene with a decrease in temperature. In contrast, 2BNG film exhibits more pronounced temperature dependence with increasing resistance at lower temperature pointing toward the semiconducting nature of the 2BNG film. Such a temperature dependence of resistance could be due to partly depleted density of states near the Fermi energy level as undoped graphene has no true band gap. However, the presence of a significant band gap of 0.2 eV, as concluded from XES-XAS measurements, can also have significant impact on the transport properties of the 2BNG film. The semiconducting behavior of hybridized BN and graphene domains have been observed previously by Li *et al.*[25] and is attributed to the presence of a small band gap. Figure 7 panels b and c show the FET $I_{ds}-V_g$ transfer characteristics of the pristine graphene and 2BNG films, respectively, carried out at different temperatures with back-gate configuration. From Figure 7b, it is observed that pristine graphene exhibits the typical ambipolar behavior with no temperature

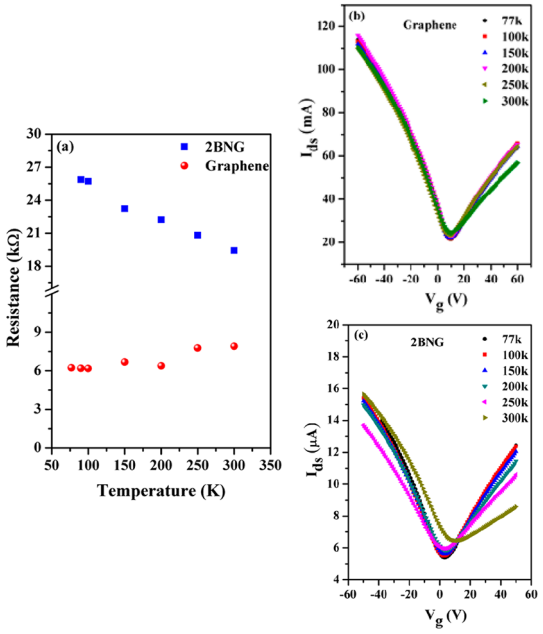

Figure 7. (a) Resistance *versus* temperature curve for pristine graphene and 2BNG film. Plot of I_{ds} as a function of V_g at V_{ds} = 1 V for back-gated FET device for (b) pristine graphene and (c) 2BNG sample at different temperatures. All measurements were carried out in a vacuum of the order of 10^{-4} mbar.

dependence at all. Interestingly, the 2BNG sample also exhibited the ambipolar behavior in the temperature range studied here (Figure 7c). As the temperature was decreased to 250 K, the point of minimum conductivity, that is, the charge neutrality point (CNP), was found to shift toward lower voltage from 10 to 3 V and did not shift with further decrease in temperature. The field effect mobility for electrons and holes deduced from the

FET curves was 12−60 $cm^2/(V \cdot s)$ in the case of the 2BNG sample which was an order of magnitude less than that of graphene. The observed decrease in mobility is quite consistent with the increase in defect density with BN doping (Table 1) which can directly affect the carrier mobility by increasing the number of scatterers.[26,35] The decrease in mobility after BN inclusion in graphene was also reported earlier by Li *et al.*,[25] and electron scattering at the boundaries between h-BN and graphene domains is resorted as a cause for the same. This is due to the purely ionic nature of bonding in h-BN with no π bands, unlike the case of the graphene lattice where electrons can move very fast owing to the presence of π bands. The ordinary mobility of B and N codoped graphene has been predicted theoretically where calculated effective mass and mobility of electrons and holes are reduced,[43] which is agreeable with the FET measurement.

CONCLUSIONS

We have successfully engineered the band gap of chemical vapor deposited graphene by *in situ* BN doping. A structural evolution in order from pure graphene, BN-doped graphene, to hybrid structure comprising h-BN and graphene domains with increasing BN concentration is observed through XPS, Raman, UV−vis, and TEM studies. A significant band gap as high as 600 meV is measured for 6% BN-doped graphene film and is attributed to the $\pi-\pi^*$ band opening of graphene due to doping of isoelectronic BN in graphene as revealed by XES and XAS studies. A reduction in mobility of the BNG is concluded due to the enhanced electron scattering of defects such as the hBN clusters, which are purely ionic in nature with no π bands. Nevertheless, a significant band gap and flexibility of varying the same in BN-doped graphene provides a remarkable leap in the development of future devices.

METHODS

Growth. As-received Cu foils supported by a quartz plate were placed into a quartz tube. The quartz tube was pumped down to a pressure of ~3 mTorr and then heated to 950 °C in 30 min in Ar flow (50 sccm) and kept at the same temperature for 30-min under Ar and H_2 flow (50/10 sccm). Meanwhile, ammonia borane was heated to 70−110 °C to obtain different BN contents. Afterward, the quartz chamber was heated to 1050 °C. CH_4 gas (10 sccm) and ammonia borane vapor, carried with Ar gas, were then introduced independently into the tube. After 15 min of growth, the system was cooled naturally to room temperature in H_2 flow.

Characterizations. The as-grown samples were characterized with XPS (VG ESCA Scientific Theta Probe) using Al K_α radiation (1486.6 eV). For TEM (JEOL JEM-2100) observation, the samples were transferred to Cu grids without assistance of polymer to avoid carbon signals from residues. Graphene and BNG films were transferred, using the conventional fishing method with poly(methyl methacrylate) (PMMA),[5] onto the substrates of SiO_2/Si wafers (300-nm-SiO_2) for Raman analysis and electrical measurements. Raman spectra were recorded using HORIBA Jobin-Yvon LabRAM H800 with both 633 nm He−Ne laser and 325 nm He−Cd laser as excitation sources. Signals from several positions on each sample were collected to confirm the uniformity of samples. Double-side polished sapphire substrates were used for optical absorption measurements. Optical absorption was measured employing the Hitachi U-4100 UV−vis−NIR spectrophotometer with Xe lamp as excitation source. Transmittance and reflectance were recorded and used for the calculation of the absorbance. Electrical properties were conducted with the cryogenic multiprobe station (LakeShore TTPX and Keithley 4200) under vacuum, and the system was cooled by liquid nitrogen for temperature-dependent experiments. Devices were put into chamber and vacuumed to 10^{-6} mbar for 1 day in order to eliminate the effect of adsorbed gas molecules on the sample surface.

C *K*-edge XAS and K_α XES measurements were carried out at beamline 8.0.1 of the Advanced Light Source, Lawrence Berkeley National Laboratory. The spectra were acquired by recording the surface sensitive total electron yield mode as a function of X-ray photon energy. The XAS spectra are normalized to the incident beam intensity, I_0, with the area under the spectra in the energy range between 317 and 320 eV fixed. The intensity of the XES spectra are normalized to the duration of data acquisition. The obtained absorption spectra have also been calibrated by the values of reference HOPG. EELS and EELS mapping were performed with a JEOL JEM-2200FS at 200 kV equipped with an omega filter.

Conflict of Interest: The authors declare no competing financial interest.

Acknowledgment. This research was financially supported by the Ministry of Education, National Science Council, Academia Sinica (Taiwan), and the Asian Office of Aerospace Research and Development under AFOSR. Technical support was provided by the Core Facilities for Nano Science and Technology, Academia Sinica, and National Taiwan University.

Supporting Information Available: Auger electron spectoscopy data for graphene transferred on SiO_2 substrate, B *K*-edge XANES spectra of 6BNG film, UV-Raman spectrum of 27% BN-doped graphene sample, Tauc's plots for pristine graphene and BN-doped graphene samples, TEM-EELS mapping images of B, C, and N for BN doped graphene samples, XPS and Raman data for BNdoped graphene samples with varying methane flow rates. This material is available free of charge *via* the Internet at http://pubs.acs.org.

REFERENCES AND NOTES

1. Novoselov, K. S.; Geim, A. K.; Morozov, S. V.; Jiang, D.; Zhang, Y.; Dubonos, S. V.; Grigorieva, I. V.; Firsov, A. A. Electric Field Effect in Atomically Thin Carbon Films. *Science* **2004**, *306*, 666–669.
2. Geim, A. K.; Novoselov, K. S. The Rise of Graphene. *Nat. Mater.* **2007**, *6*, 183–191.
3. Novoselov, K. S.; Geim, A. K.; Morozov, S. V.; Jiang, D.; Katsnelson, M. I.; Grigorieva, I. V.; Dubonos, S. V.; Firsov, A. A. Two-Dimensional Gas of Massless Dirac Fermions in Graphene. *Nature* **2005**, *438*, 197–200.
4. Bolotin, K. I.; Ghahari, F.; Michael, D.; Shulman, M. D.; Stormer, H. L.; Kim, P. Observation of The Fractional Quantum Hall Effect in Graphene. *Nature* **2009**, *462*, 196–199.
5. Cheng, R.; Bai, J.; Liao, L.; Zhou, H.; Chen, Y.; Liu, L.; Lin, Y. C.; Jiang, S.; Huang, Y.; Duan, X. High-Frequency Self-Aligned Graphene Transistors with Transferred Gate Stacks. *Proc. Nat. Acad. Sci.* **2012**, *109*, 11588–11592.
6. Wu, Y.; Jenkins, K. A.; Alberto, V. G.; Farmer, D. B.; Zhu, Y.; Bol, A. A.; Dimitrakopoulos, C.; Zhu, W.; Xia, F.; Avouris, P.; *et al.* State-of-the-Art Graphene High Frequency Electronics. *Nano Lett.* **2012**, *12*, 3062–3067.

7. Bonaccorso, F.; Hasan, T.; Ferrari, A. C. Graphene Photonics and Optoelectronics. *Nat. Photon.* **2010**, *4*, 611–622.
8. Dlubak, B.; Martin, M. B.; Deranlot, C.; Servet, B.; Xavier, S.; Mattana, R.; Sprinkle, M.; Berger, C.; De Heer, W. A.; Petroff, F.; *et al*. Highly Efficient Spin Transport in Epitaxial Graphene on SiC. *Nat. Phys.* **2012**, *8*, 557–561.
9. Son, Y.-N.; Lohen, M. L.; Louie, S. G. Energy Gaps in Graphene Nanoribbons. *Phys. Rev. Lett.* **2006**, *97*, 216803.
10. Shemella, P.; Zhang, Y.; Mailman, M.; Ajayan, P. M.; Nayak, S. K. Energy Gaps in Zero-Dimensional Graphene Nanoribbons. *Appl. Phys. Lett.* **2007**, *91*, 042101.
11. Linden, S.; Zhong, D.; Timmer, A.; Aghdassi, N.; Franke, J. H.; Zhang, H.; Feng, X.; Mullen, K.; Fuchs, H.; Chi, L.; *et al*. Electronic Structure of Spatially Aligned Graphene Nanoribbons on Au(788). *Phys. Rev. Lett.* **2012**, *108*, 216801.
12. Zhang, Y. B.; Tang, T. T.; Girit, C.; Hao, Z.; Martin, M. C.; Zettl, A.; Crommie, M. F.; Shen, Y. R.; Wang, F. Direct Observation of a Widely Tunable Bandgap in Bilayer Graphene. *Nature* **2009**, *459*, 820–823.
13. Shi, Y.; Kim, K. K.; Relna, A.; Hofmann, M.; Li, L. J.; Kong, J. Work Function Engineering of Graphene Electrode *via* Chemical Doping. *ACS Nano* **2010**, *4*, 2689–2694.
14. Casolo, S.; Martinazzo, R.; Tantardini, G. F. Band Engineering in Graphene with Superlattices of Substitutional Defects. *J. Phys. Chem. C* **2011**, *115*, 3250–3256.
15. Usachov, D.; Vilkov, O.; Gruneis, A.; Haberer, D.; Fedorov, A.; Adamchuk, V. K.; Preobrajenski, A. B.; Dudin, P.; Barinov, A.; Oehzelt, M.; *et al*. Nitrogen-Doped Graphene: Efficient Growth, Structure, and Electronic Properties. *Nano Lett.* **2011**, *11*, 5401–5407.
16. Naumov, I. I.; Bratkovsky, A. M. Gap Opening in Graphene by Simple Periodic Inhomogeneous Strain. *Phys. Rev. B* **2011**, *84*, 245444.
17. Lu, Y.; Guo, J. Band Gap of Strained Graphene Nanoribbons. *Nano Res.* **2010**, *3*, 189–199.
18. Shinde, P. P.; Kumar, V. Direct Band Gap Opening in Graphene by BN Doping: *Ab Initio* calculations. *Phys. Rev. B* **2011**, *84*, 125401.
19. Martins, J. D.; Chacham, H. Disorder and Segregation in B−C−N Graphene-type Layers and Nanotubes: Tuning the Band Gap. *ACS Nano* **2011**, *5*, 385–393.
20. Tachikawa, H.; Iyama, T.; Azumi, K. Density Functional Theory Study of Boron- and Nitrogen-Atom-Doped Graphene Chips. *Jpn. J. Appl. Phys.* **2011**, *50*, 01BJ03.
21. Xu, B.; Lu, Y. H.; Feng, Y. P.; Lin, J. Y. Density Functional Theory Study of BN-Doped Graphene Superlattice: Role of Geometrical Shape and Size. *J. Appl. Phys.* **2010**, *108*, 073711.
22. Yu, S.; Zheng, W.; Wang, C.; Jiang, Q. Nitrogen/Boron Doping Position Dependence of the Electronic Properties of a Triangular Graphene. *ACS Nano* **2011**, *5*, 385–393.
23. Song, L.; Ci, L.; Lu, H.; Sorokin, P. B.; Jin, C.; Ni, J.; Kvashnin, A. G.; Kvashnin, D. G.; Lou, J.; Yakobson, B. I.; *et al*. Large Scale Growth and Characterization of Atomic Hexagonal Boron Nitride Layers. *Nano Lett.* **2010**, *10*, 3209–3215.
24. Shi, Y.; Hamsen, C.; Jia, X.; Kim, K. K.; Reina, A.; Hofmann, M.; Hsu, A. L.; Zhang, K.; Li, H.; Juang, Z.-Y.; *et al*. Synthesis of Few-Layer Hexagonal Boron Nitride Thin Film by Chemical Vapor Deposition. *Nano Lett.* **2010**, *10*, 4134–4139.
25. Ci, L.; Song, L.; Jin, C.; Jariwala, D.; Wu, D.; Li, Y.; Srivastava, A.; Wang, Z. F.; Storr, K.; Balicas, L.; *et al*. Atomic Layers of Hybridized Boron Nitride and Graphene Domains. *Nat. Mater.* **2010**, *9*, 430–435.
26. Hwang, J. Y.; Kuo, C. C.; Chen, L. C.; Chen, K. H. Correlating Defect Density with Carrier Mobility in Large-Scaled Graphene Films: Raman Spectral Signatures for the Estimation of Defect Density. *Nanotechnology* **2010**, *21*, 465705.
27. Lei, W.; Portehault, D.; Dimova, R.; Antonietti, M. Boron Carbon Nitride Nanostructures from Salt Melts: Tunable Water Soluble Phosphors. *J. Am. Chem. Soc.* **2011**, *133*, 7121–7127.
28. Kawaguchi, M. B/C/N Materials Based on the Graphite Network. *Adv. Mater.* **1997**, *9*, 615–625.
29. Ozaki, J.; Kimura, N.; Anahara, T.; Oya, A. Preparation and Oxygen Reduction Activity of BN Doped Carbons. *Carbon* **2007**, *45*, 1847–1853.
30. Ismach, A.; Chou, H.; Ferrer, D. A.; Wu, Y.; Mcdonnell, S.; Floresca, H. C.; Covacevich, A.; Pope, C.; Piner, R.; Kim, M. J.; *et al*. Towards the Controlled Synthesis of Hexagonal Boron Nitride Films. *ACS Nano* **2012**, *6*, 6378–6385.
31. Moulder, J.; Stickle, W.; Sobol, P.; Bomben, K., *Handbook of X-ray Photoelectron Spectroscopy*; Physical Electronics, Inc.: Eden Prairie, Minnesota, USA, 1995.
32. Panchakarla, L. S.; Subrahmanyam, K. S.; Saha, S. K.; Govindraj, A.; Krishnamurthy, H. R.; Waghmare, U. V.; Rao, C. N. R. Synthesis, Structure, and Properties of Boron- and Nitrogen-Doped Graphene. *Adv. Mater.* **2009**, *21*, 4726–4730.
33. Ferrari, A. C. Raman Spectroscopy of Graphene and Graphite: Disorder, Electron-Phonon Coupling, Doping and Nonadiabatic Effects. *Solid State Commun.* **2007**, *143*, 47–57.
34. Cancado, L. G.; Jorio, A.; Martins Ferreira, E. H.; Stavale, F.; Achete, C. A.; Capaz, R. B.; Moutinho, M. V. O.; Lombardo, A.; Kulmala, T. S.; Ferrari, A. C. Quantifying Defects in Graphene *via* Raman Spectroscopy at Different Excitation Energies. *Nano Lett.* **2011**, *11*, 3190–3196.
35. Ni, Z. H.; Ponomarenko, L. A.; Nair, R. R.; Yang, R.; Anissimova, S.; Grigorieva, I. V.; Schedin, F.; Blake, P.; Shen, Z. X.; Hill, E. H.; *et al*. On Resonant Scatterers as a Factor Limiting Carrier Mobility in Graphene. *Nano Lett.* **2010**, *10*, 3868–3872.
36. Reich, S.; Ferrari, A. C. Resonant Raman Scattering in Cubic and Hexagonal Boron Nitride. *Phys. Rev. B* **2005**, *71*, 205201.
37. Yang, L.; Deslippe, J.; Park, C.-H.; Cohen, M. L.; Louie, S. G. Excitonic Effects on The Optical Response of Graphene and Bilayer Graphene. *Phys. Rev. Lett.* **2009**, *103*, 186802.
38. Frueh, S.; Kellett, R.; Mallery, C.; Molter, T.; Willis, W. S.; King'ondu, C.; Suib, S. L. Pyrolytic Decomposition of Ammonia Borane to Boron Nitride. *Inorg. Chem.* **2011**, *50*, 783–792.
39. Kim, K. K.; Hsu, A.; Jia, X.; Kim, S. M.; Shi, Y.; Hofmann, M.; Nezich, D.; Rodriguez-Nieva, J. F.; Dresselhaus, M.; Palacios, T.; *et al*. Synthesis of Monolayer Hexagonal Boron Nitride on Cu Foil Using Chemical Vapor Deposition. *Nano Lett.* **2012**, *12*, 161–166.
40. Marins, J. R.; Chacham, H. N-rich B−C−N Layers: From Segregated Alloy to Solid Solution. *Phys. Rev. B* **2012**, *86*, 075421.
41. Brito, W. H.; Kagimura, R.; Miwa, R. H. B and N Doping in Graphene Ruled by Grain Boundary Defects. *Phys. Rev. B* **2012**, *85*, 035404.
42. Sutter, P.; Cortes, R.; Lahiri, J.; Sutter, E. Interface Formation in Monolayer Graphene−Boron Nitride Heterostructures. *Nano Lett.* **2012**, 10.1021/nl302398m.
43. Liu, L.; Shen, Z. Bandgap Engineering of Graphene: A Density Functional Theory Study. *Appl. Phys. Lett.* **2009**, *95*, 252104.